



Scanning tunneling spectroscopy of gold nanoparticles: Influences of volatile organic vapors and particle core dimensions

Li-Ping Xu, Shaowei Chen *

Department of Chemistry and Biochemistry, University of California, 1156 High Street, Santa Cruz, CA 95064, United States

ARTICLE INFO

Article history:

Received 27 October 2008

In final form 2 December 2008

Available online 10 December 2008

ABSTRACT

Scanning tunneling spectroscopy of hexanethiolate-protected gold nanoparticles was studied in the presence of volatile organic vapors. The particles were immobilized onto a Au(111) surface that was modified with a hexanethiol self-assembled monolayer. It was found that particle dimensions played a critical role in dictating the STS behaviors in response to exposure to organic vapors, with the optimal core diameter around 4.9 nm. This was interpreted on the basis of solvent penetration into the nanoparticle/self-assembled monolayer interface and the resulting manipulation of nanojunction capacitance and resistance. These fundamental insights may be exploited as a sensing mechanism for chemical vapor detection.

© 2008 Elsevier B.V. All rights reserved.

1. Introduction

Vapor sensors have gained tremendous attention due to their potential applications in medical diagnostics, homeland security, and environmental monitoring [1–8]. Of these, chemiresistive sensors are those based on materials whose conductivity changes in the presence of a volatile vapor, with the typical active ingredients consisting of metal oxides, nanowires, nanotubes, and nanoparticles [9–17]. This type of sensors may be easily miniaturized and highly portable. For instance, previous studies have demonstrated the viability of using monolayer-encapsulated gold nanoparticles as the sensitive coatings [1,2,4,11,18] in the development of novel chemical sensors. The sensing mechanism is based on chemical manipulation of charge transport between the metal cores where the alkanethiolate layer serves as the electron tunneling barrier [16,19]. It is presumed that the sorption of chemical vapors into the organic matrix leads to swelling of the interparticle organic shell. Consequently, the electronic conductance of the particle ensemble decreases because of enhanced particle separation that impedes interparticle electron hopping. So far, the majority of these studies have been focused on ensemble average of a dropcast thick film where rampant structural defects may render it difficult to establish an unambiguous correlation between the nanoparticle structures and vapor detection sensitivity. In contrast, scanning tunneling spectroscopy (STS) allows the evaluation of the charge transfer properties of individual nanoparticles of specific and varied size, which makes it possible to directly correlate the tunneling characteristics in a specific chemical environment with particle molecular structures. The fundamental insights may thus be

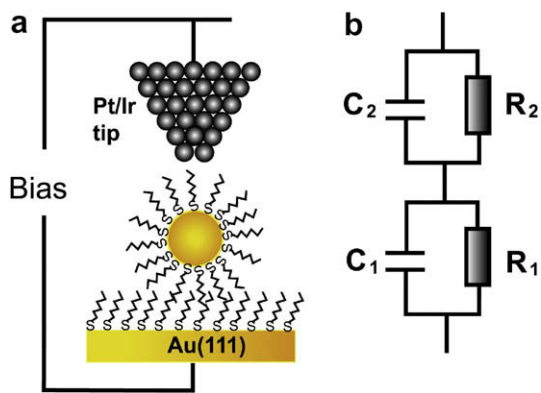
exploited as a novel sensing mechanism for chemical vapor detection. This is the primary motivation of the present work.

In STS measurements, both Coulomb blockade and Coulomb staircase phenomena may be observed [20–22], when two pre-requisites are satisfied [23]. First, to observe single electron tunneling of an isolated metallic nanoparticle of capacitance (C), the energy associated with transferring one electron ($E_c = e^2/2C$, where e is the elementary charge unit) must exceed thermal kinetic energy ($k_B T$). At room temperature ($k_B T = 26$ meV), this dictates that the metal nanoparticle size must be below 10 nm so that the capacitance is on the order of 10^{-18} F. Second, the electrical contacts to the particles must have tunneling resistance larger than the quantum resistance ($h/4e^2 \sim 6.5$ k Ω), in order to suppress quantum fluctuations of the electron charge. Notably, the features of Coulomb staircase and Coulomb blockade are both sensitive to the structure of the nanoparticle as well as the nanoscale chemical environments; thus, they may be exploited as sensing mechanisms for chemical detection. To this end, in combination with scanning tunneling microscopy (STM), STS offers a unique opportunity to examine the charge transfer characteristics of selected nanoparticles in a controlled environment [24–30]. Here, the tip–substrate interface can be modeled by a double barrier tunneling junction (DBTJ), which is shown in Scheme 1 [20]. One junction is formed between the nanoparticle and the STM tip, and the other between the metal nanoparticle and the conductive substrate.

In this Letter, using hexanethiolate-protected gold nanoparticles as the illustrating example, we will examine the effects of nanoparticle core size and volatile organic vapors on the corresponding STS characteristics. The charge transfer properties will be examined within the context of the correlation between nanoparticle solvation and nanojunction resistance and capacitance. The results suggest that there exists an optimal particle core dimension for chemical vapor detection, as reflected by the

* Corresponding author. Fax: +1 831 459 2935.

E-mail address: schen@chemistry.ucsc.edu (S. Chen).



Scheme 1. (a) Schematic of a DBTJ setup formed by an STM tip, a ligand-stabilized gold particle, and a Au substrate. (b) Corresponding equivalent circuit of the DBTJ structure.

variation of the Coulomb blockade gap with vapor concentration and polarity. These interfacial characteristics may serve as a fundamental basis for chemical sensing.

2. Experiment

2.1. Materials

Hydrogen tetrachloroauric acid (HAuCl_4) was synthesized by dissolving ultra-high purity gold (99.999%, Johnson Matthey) in freshly prepared aqua regia followed by crystallization. Tetra-*n*-octylammonium bromide (Alfa Aesar, 98%), *n*-hexanethiol (C6SH, Acros, 96%), sodium borohydride (NaBH_4 , Acros, 99%) were all used as received. Solvents were purchased from typical commercial sources at their highest purities and used without further treatments. Water was supplied by a Barnstead Nanopure water system (18.3 $\text{M}\Omega\text{ cm}$). Hexanethiolate-protected gold (AuC6) nanoparticles were synthesized by using the modified Brust protocol [31].

2.2. STM/STS measurements

Au(111) thin films supported on mica were purchased from Molecular Imaging Inc. Prior to use, the gold surfaces were subject to UV-ozone (Model 42, Jelight Co.) cleaning for 10 min. Then the gold substrates were immersed into a 1 mM solution of hexanethiol (C6SH) in ethanol for 24 h to form a self-assembled monolayer (SAM). The samples for STM/STS measurements were then prepared by dropcasting a dilute solution of the AuC6 nanoparticles in toluene onto the C6SH SAM-modified Au(111) substrate, followed by solvent evaporation at ambient temperature. STM and STS measurements were carried out using a PicoLE SPM instrument (Molecular Imaging), operated at room temperature in air or in a controlled atmosphere. Mechanically cut Pt/Ir wires were used as the tips in the entire measurements. A high impedance of 75 $\text{M}\Omega$ (bias 1.5 V and set point 0.02 nA) was used to prevent tip damage or capture of the metal particles. All STM topographic images were recorded in constant current mode. The corresponding I - V data were collected in the spectroscopy mode when the feedback loop was turned off. Large areas of $\sim 200\text{ nm}^2$ were scanned first to locate isolated nanoparticles; then stable images were acquired by zooming into smaller areas. At least 200 I - V data points were collected in a typical voltage sweep of $\pm 2\text{ V}$, and every I - V curve was averaged for five times.

To examine the effects of volatile organic vapors on the STS properties of the nanoparticles, the STS spectra were collected by injecting calculated amounts of different solvents into the environ-

mental chamber with a Hamilton microliter syringe. Nitrogen was used to purge the chamber between injections. Particles of three different core sizes were selected for the measurements. Control experiments with the C6SH SAM were also carried out under the same conditions.

3. Results and discussion

As mentioned above, the AuC6 particles were immobilized onto a C6SH SAM-modified Au(111) surface. Because of the intercalation between the hexanethiolate protecting ligands and the alkyl chains of the C6SH SAM, stable and reproducible images of the AuC6 nanoparticles were obtained even after repetitive scans [20]. STS current-voltage (I - V) measurements were then carried out by parking the Pt/Ir tip over selected particles with the feedback loop switched off.

Three particles were selected for the STS studies with the size varied from 3.2 nm to 6.3 nm and 11.8 nm (corresponding to a core diameter of 1.8 nm, 4.9 nm, and 10.4 nm, respectively, considering that the fully extended chain length of hexanethiolate is 0.77 nm, as evaluated by Hyperchem[®] calculations). A control experiment was also carried out by moving the STM tip to a random spot directly over the C6SH SAM. Typically in STS measurements, with the application of a bias voltage across the nanojunction (Scheme 1), when the junction capacitance is small enough and hence the charging energy is big enough, no apparent charge transport occurs across the junction within a certain range of bias voltages, the so-called Coulomb blockade phenomenon. Beyond this threshold region, the electron energy is high enough to overcome the charging energy and hence appreciable tunneling current is detected, where the discrete charge transfer events are reflected as the Coulomb staircase features. The introduction of volatile organic vapors into the nanojunction is anticipated to drastically impact the overall STS responses as both the junction capacitances and resistances may be varied because of vapor solvation.

In the present study, hexane was chosen as an initial representative example. Experimentally, a calculated amount of hexane was injected into the environmental chamber of the STM instrument, and the STS spectra were then collected. Fig. 1 depicts the STS responses of three AuC6 particles in nitrogen and in the presence of different concentration of hexane (note that as mentioned in Section 2, the chamber was purged with ultrahigh-purity nitrogen between injections), which exhibited a clear variation with the particle dimension. For the smallest particle (panel a, diameter 3.2 nm), whereas the variation of the Coulomb blockade gap with the concentration of the hexane vapor was somewhat scattering (most probably because of the small particle core size and consequently the difficulty of maintaining the STM tip at the same position on top of the particle), statistical analysis based on more than 10 independent measurements showed that initially in N_2 the particle exhibited a Coulomb gap of ca. 0.86 V, which increased slightly with increasing concentration of hexane, as manifested by the black line in Fig. 2. For instance, at a hexane concentration of 4–5 mM, the width of the Coulomb blockade increased to about 1.1 V. For the particle of 6.3 nm in diameter (Fig. 1b), initially in N_2 , there was no apparent Coulomb gap, whereas in 5 mM of hexane vapors, the gap increased rapidly to ca. 2.53 V, as shown by the red¹ line in Fig. 2. In sharp contrast, for the largest particles (panel c, Fig. 1, 11.8 nm in diameter), no obvious difference in the I - V responses was observed in nitrogen and in hexane vapor. Even in the presence of up to 5 mM of hexane, very well-defined Coulomb

¹ For interpretation of color in Fig. 2, the reader is referred to the web version of this article.

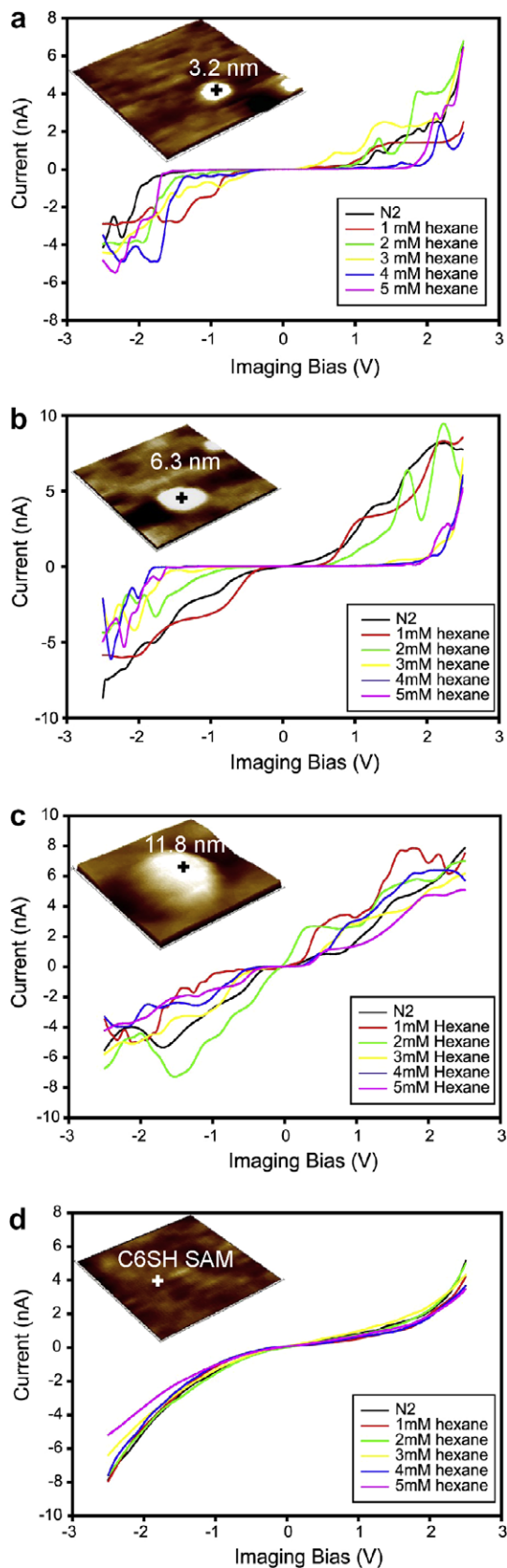


Fig. 1. (a) Scanning tunneling spectroscopy of Au6 nanoparticles of varied core diameters in different concentrations of hexane. The STM topographic images of the particles were shown in the corresponding insets: (a) 3.2 nm; (b) 6.3 nm; and (c) 11.8 nm. Control experiments with the hexanethiol SAM-modified Au(111) substrate are shown in panel (d).

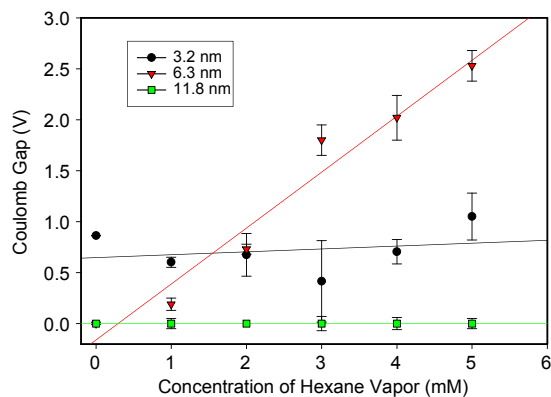


Fig. 2. Variation of the Coulomb gap with hexane concentration for three different particles. Data were obtained from I - V measurements exemplified in Fig. 1. Error bars were standard deviations based on >10 independent measurements.

staircase features can still be seen with no apparent blockade gap (green line, Fig. 2).

The different STS responses may be accounted for by the penetration of the hexane vapor into the particle protecting shell and C6SH SAM and the effect of solvation by this low-dielectric solvent medium on the junction capacitance and resistance. It is generally believed that the overall junction capacitance ($C_t = C_1 + C_2$) will decrease and concurrently the resistance ($R_1 + R_2$) increases upon the exposure to a low-dielectric organic vapor. However, because of the metal–organic composite nature of the nanoparticles, the impact of vapor solvation on the junction charge transport properties is anticipated to vary with the nanoparticle structure (and hence particle capacitance). For very small particles (Fig. 1a), the high charging energy ($e^2/2C$) leads to low conductance of the junction, and the effect of vapor penetration into the particle/SAM interface on the junction conductance is expected to diminish at a sufficiently high bias. Thus, only a small increment of the Coulomb gap was observed experimentally (Fig. 2). For very large particles (e.g. Fig. 1c), the large particle core (and capacitance) renders the junction very conductive with no apparent Coulomb gap, and the solvation of the particle/SAM interface did not increase the charging energy ($e^2/2C$) significantly enough to hinder completely the charge transport across the junction even at zero bias. Therefore, no substantial variation of the junction conductivity was found. For particles of intermediate size (e.g. Fig. 1b), however, the junction conductivity becomes readily controllable with the variation of the junction capacitance and resistance by virtue of vapor solvation. Here the solvation of the particle protecting layer (and the C6SH SAM) by a low-dielectric solvent leads to an increase of the resistance (R_1) and decrease of the capacitance (C_1) of junction 1 (Scheme 1). Such a swelling effect results in the widening of the junction Coulomb gap, as observed experimentally above (Fig. 2).

To confirm that the observed variation of STS responses was indeed due to the solvation effects on nanoparticle charge transfer, a control experiment was carried out by parking the STM tip on the C6SH SAM surface. STS measurements in the presence of different concentrations of hexane showed only featureless and almost invariant profiles (Fig. 1d), where the sigmoidal-shaped curves for C6SH SAM/Au(111) is consistent with those observed previously [32].

The above studies suggest that the charge transport properties of Au6 nanoparticles of 6.3 nm in diameter exhibit the most sensitive variation with volatile organic vapors. Thus, these particles were selected for further studies in the detection of other organic vapors, which spanned a rather wide range of relative polarity, including hexane (0.009), toluene (0.099), ethyl ether (0.117),

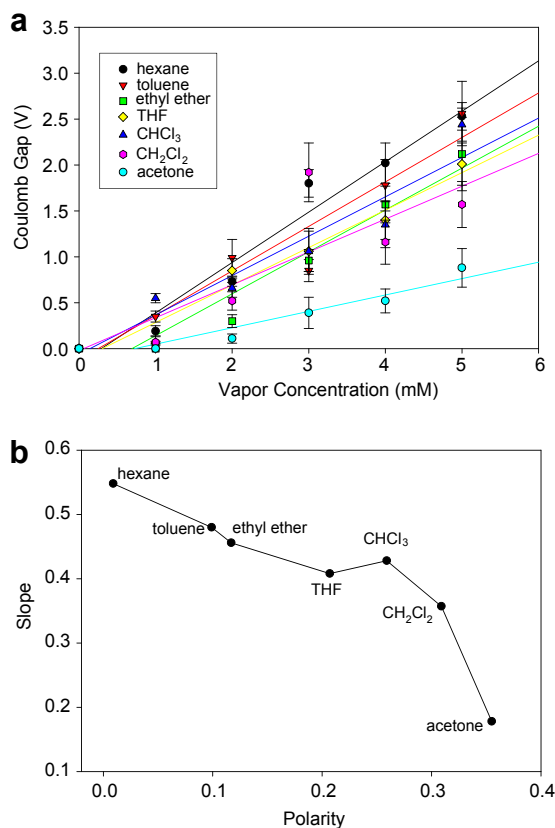


Fig. 3. (a) Variation of the STS Coulomb gaps of AuC6 nanoparticles (diameter 6.3 nm) with volatile solvents of different concentrations. Symbols are experimental data, and lines are linear regressions, the slopes of which were plotted in panel (b) as a function of the relative polarity of the organic solvents.

tetrahydrofuran (THF, 0.207), chloroform (CHCl₃, 0.259), dichloromethane (DCM, 0.309), and acetone (0.355) [33]. Fig. 3a depicts the growth of the Coulomb blockade gap of the AuC6 particle (6.3 nm in diameter, same as in Fig. 1b) with the concentration of these different volatile vapors, and the general trend is that the Coulomb gaps all enlarged with increasing vapor concentration. Importantly, the sensitivity of the increase of the Coulomb gap with vapor concentration appears to be correlated directly to the polarity of the vapor, which is shown in Fig. 3b. That is, the less polar the organic vapor, the more significant impact on the particle Coulomb blockade gap. In particular, for solvents with relative polarity lower than 0.25, the widening of the Coulomb gap with vapor concentration is much more drastic than that for the more polar solvents. As these particles have been well-known to be soluble in apolar solvents such as hexane, toluene, ethyl ether, THF, CHCl₃, and CH₂Cl₂, but not in polar solvents such as acetone and alcohols, the evolution of the Coulomb gap with the nature of organic vapors may be accounted for by the solvation effect on junction capacitance and resistance. Note that as solvent penetrates into the particle protecting layer, the ligands would exhibit increasingly disordered (*gauche*) conformations, which would become more pronounced with less polar solvents, rendering the through-bond charge transport less efficient and hence enhanced junction impedance [34].

4. Conclusion

In this study, the STS behaviors of AuC6 nanoparticles of different sizes were examined at room temperature. For small gold par-

ticles (ca. 3 nm in diameter) in nitrogen, the particles exhibited a relatively large Coulomb blockade region which increased slightly upon the introduction of varied concentrations of volatile organic vapors. For very large particles with a diameter of ca. 12 nm, obvious staircases were observed in the *I*-*V* measurements with no apparent Coulomb gap, and the features remained practically unchanged upon exposure to different organic vapors. In sharp contrast, for AuC6 nanoparticles that are around 6 nm in diameter (core diameter ca. 4.9 nm), the *I*-*V* profiles exhibited a rather sensitive variation upon the exposure to varied organic vapors, reflected by a drastic enlargement of the Coulomb gap with increasing vapor concentration and decreasing vapor relative polarity. The differences of these experimental observations may be accounted for by the effects of particle structure and vapor solvation on the particle charging energy ($e^2/2C$) which dictates charge transport across the tip/particle/substrate junction. Specifically, for very small particles, swelling of the particle/SAM interface by organic vapors might lead to diminishment of the already low junction conductance; yet the impact is anticipated to be small and might be partially overcome by the applied bias. For very large particles, exposure to organic vapors is anticipated to also lower the junction conductance; yet the large particle core size dictates that charge transfer may still occur even at zero bias. The results suggest that there exists an optimal range of particle size where the particles exhibit most sensitive variation to volatile organic vapors. This may serve as a fundamental basis in the development of nanoparticle-based chemiresistors for chemical vapor detection.

Acknowledgment

This work was supported in part by the National Science Foundation (CHE-0718190).

References

- [1] H. Ahn, A. Chandekar, B. Kang, C. Sung, J.E. Whitten, *Chem. Mater.* 16 (2004) 3274.
- [2] J.W. Grate, D.A. Nelson, R. Skaggs, *Anal. Chem.* 75 (2003) 1868.
- [3] L. Han, D.R. Daniel, M.M. Maye, C.J. Zhong, *Anal. Chem.* 73 (2001) 4441.
- [4] C.Y. Yang, C.L. Li, C.J. Lu, *Anal. Chim. Acta* 565 (2006) 17.
- [5] W. Gopel, C. Ziegler, H. Breer, D. Schild, R. Apfelbach, J. Joerges, R. Malaka, *Biosens. Bioelectron.* 13 (1998) 479.
- [6] A.K. Pavlou, A.P.F. Turner, *Clin. Chem. Lab. Med.* 38 (2000) 99.
- [7] D.J. Strike, M.G.H. Meijerink, M. Koudelka-Hep, *Fresenius J. Anal. Chem.* 364 (1999) 499.
- [8] J. Yinon, *Anal. Chem.* 75 (2003) 99A.
- [9] K.J. Albert, N.S. Lewis, C.L. Schauer, G.A. Sotzing, S.E. Stitzel, T.P. Vaid, D.R. Walt, *Chem. Rev.* 100 (2000) 2595.
- [10] R. Dutta, E.L. Hines, J.W. Gardner, K.R. Kashwan, A. Bhuyan, *Sens. Actuators B: Chem.* 94 (2003) 228.
- [11] Y. Joseph et al., *J. Phys. Chem. B* 107 (2003) 7406.
- [12] N.S. Lewis, *Acc. Chem. Res.* 37 (2004) 663.
- [13] Q.F. Pengfei et al., *NanoLetters* 3 (2003) 347.
- [14] N. Krasteva, I. Besnard, B. Guse, R.E. Bauer, K. Mullen, A. Yasuda, T. Vossmeier, *NanoLetters* 2 (2002) 551.
- [15] E.C. Walter, F. Favier, R.M. Penner, *Anal. Chem.* 74 (2002) 1546.
- [16] F.P. Zamborini, M.C. Leopold, J.F. Hicks, P.J. Kulesza, M.A. Malik, R.W. Murray, *J. Am. Chem. Soc.* 124 (2002) 8958.
- [17] H.L. Zhang, S.D. Evans, J.R. Henderson, R.E. Miles, T.H. Shen, *Nanotechnology* 13 (2002) 439.
- [18] A.W. Snow, H. Wohltjen, *Chem. Mater.* 10 (1998) 947.
- [19] W.P. Wuelfing, S.J. Green, J.J. Pietron, D.E. Cliffler, R.W. Murray, *J. Am. Chem. Soc.* 122 (2000) 11465.
- [20] G.H. Yang, L. Tan, Y.Y. Yang, S.W. Chen, G.Y. Liu, *Surf. Sci.* 589 (2005) 129.
- [21] S. Pradhan, J. Sun, F.J. Deng, S.W. Chen, *Adv. Mater.* 18 (2006) 3279.
- [22] S.W. Chen et al., *Science* 280 (1998) 2098.
- [23] K.K. Likharev, *IBM J. Res. Dev.* 32 (1988) 144.
- [24] O. Millo, D. Katz, Y. Levi, Y.W. Cao, U. Banin, *J. Low Temp. Phys.* 118 (2000) 365.
- [25] D. Steiner, A. Aharoni, U. Banin, O. Millo, *NanoLetters* 6 (2006) 2201.
- [26] C.A. Nijhuis, N. Oncel, J. Huskens, H.J.W. Zandvliet, B.J. Ravoo, B. Poelsema, D.N. Reinhoudt, *Small* 2 (2006) 1422.
- [27] V. Jacobsen, T. Zhu, W. Knoll, M. Kreiter, *Eur. J. Inorg. Chem.* (2005) 3683.
- [28] P. Jiang, Z.F. Liu, S.M. Cai, *J. Appl. Phys.* 90 (2001) 2039.
- [29] U. Banin, Y.W. Cao, D. Katz, O. Millo, *Nature* 400 (1999) 542.

- [30] A.M. Jackson, J.W. Myerson, F. Stellacci, *Nat. Mater.* 3 (2004) 330.
- [31] M. Brust, M. Walker, D. Bethell, D.J. Schiffrin, R. Whyman, *J. Chem. Soc.: Chem. Commun.* (1994) 801.
- [32] L.A. Bumm et al., *Science* 271 (1996) 1705.
- [33] C. Reichardt, *Solvents and Solvent Effects in Organic Chemistry*, third edn., Wiley-VCH, Weinheim, 2003.
- [34] M. Fujihira, M. Suzuki, S. Fujii, A. Nishikawa, *Phys. Chem. Chem. Phys.* 8 (2006) 3876.